

## Supplementary Materials

### **Quinone-based imide conjugated microporous polymer-reductive graphene oxide composite as an efficient electrode for hybrid supercapacitor**

Yuyu Dai, Yue Gao, Haoran Xu, Xiaoqing Li, Xiangsheng Xu, Zhenming Li\*

*College of Chemical Engineering, Zhejiang University of Technology, Hangzhou,  
310014, P. R. China. E-mail: lizmzf@163.com*

## **Contents**

- 1. Materials**
- 2. Methods**
- 3. Synthesis of TABQ monomer**
- 4. Calculations of capacitive characteristics**
- 5. Electrochemical properties of PIBQ polymer**
- 6. Peak current diagram and capacitive contribution of PIBT-1%rGO composite**
- 7. Cycling stability of PIBQ-1%rGO composite**
- 8. FT-IR characterization of PIBT-1%rGO composite**
- 9. EIS diagram of PIBQ polymer, PIBT-1%rGO and PIBQ-1%rGO composite**
- 10. EIS diagram of PIBQ-1%rGO//PIBQ-1%rGO device**
- 11. Reference**

## 1. Materials

1,4,5,8-naphthalene-tetracarboxylic acid dianhydride (NTCDA), 1,2,4,5-benzenetetraamine tetrahydrochloride (BT) were purchased from admas-beta.

Monolayer graphene oxide dispersion (0.5 g/mL) was purchased from XFNANO (Nanjing). 2,3,5,6-tetraaminocyclohexa-2,5-diene-1,4-dione (TABQ) was prepared by us according to the corresponding literatures. All solvents, reagents and chemicals were purchased from general-reagent and used without further purification.

## 2. Methods

$^1\text{H}$  (500MHz) NMR spectra of the synthesized compounds were recorded on Bruker AVANCE 111 instrument (Bruker, Switzerland).

MALDI time-of-flight mass spectrometry (MALDI-TOF-MS) analysis was tested using an AXIMA-CFRTM plus instrument.

The groups of the samples were characterized using Fourier transform infrared spectroscopy (FT-IR, Nicolet-6700, USA).

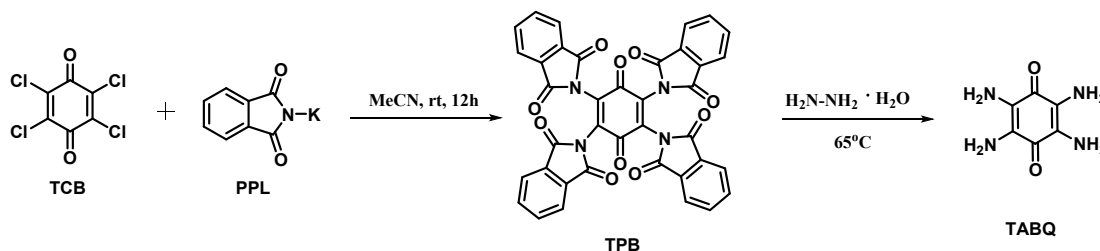
The surface morphology of the material was carried out by Zeiss scanning electron microscope (Germany).

TEM was taken on a 120kv transmission electron microscope with an accelerating voltage of 200 kV. Before being transferred into the TEM chamber, the samples dispersed in ethanol were deposited onto holey carbon films supported on Cu grids.

### 3. Synthesis of TABQ monomer

The synthesis of 2,3,5,6-tetra (amino) p-benzoquinone (TABQ) was divided into two steps, as shown in **Scheme 1** according to the literature.<sup>[1]</sup> The anhydrous acetonitrile (50 mL) solvent was added into the three necked flask containing tetrachlorobenzoquinone (TCB, 5 g) and potassium phthalimide (PPL, 15 g) under nitrogen atmosphere. Then, the resulting mixture was stirred and heated at 80 °C for 12 h. After the reaction finished, the reaction mixture was cooled to room temperature and filtered, and the residue was washed with N, N-dimethylformamide (DMF) and H<sub>2</sub>O at 100 °C for three times. After that, the residue was added into the absolute ethanol and the suspended solution was heated until boiling, and immediately filtered. A yellow solid powder (TPB) (5.73 g) was obtained after drying the solid under vacuum condition.

The second step is that hydrazine hydrate (50%, 26 mL) was added into the round-bottom flask containing TPB (5.73 g), and the mixture solution was reacted at 65 °C for 2 h. A purple solid product 2,3,5,6-tetra (amino) p-benzoquinone (TABQ) was obtained after the reaction solution was washed with H<sub>2</sub>O and absolute ethanol for three times. <sup>1</sup>H NMR (600 MHz, DMSO-*d*<sub>6</sub>) δ 4.55 (s, 8H).



**Scheme S1** Synthetic route of 2,3,5,6-tetra (amino) p-benzoquinone (TABQ)

#### 4. Calculations of capacitive characteristics

For the three electrode configuration, the gravimetric specific capacitance ( $C_w$ ) was calculated based on the following equation:

$$C_w = \frac{I \times \Delta t}{m} \quad (1)$$

Where 'I' is current (A), ' $\Delta t$ ' is discharge cycle time (s), 'm' is mass of active material (g).

For the two-electrode configuration (device measurements), the capacitance is calculated by the above formula but 'm' is replaced by 'M', which is the mass of the overlapping portion of the two electrode pads (g).

The energy density and power density of the materials were obtained from the equations:

$$E = \frac{1}{2} \times C_w \times \Delta V^2 \quad (2)$$

$$P = \frac{E}{\Delta t} \times 3600 \quad (3)$$

Where ' $E$ ' is energy density ( $\text{W h kg}^{-1}$ ) ' $P$ ' is the power density ( $\text{W kg}^{-1}$ ).

## 5. Electrochemical properties of PIBQ polymers

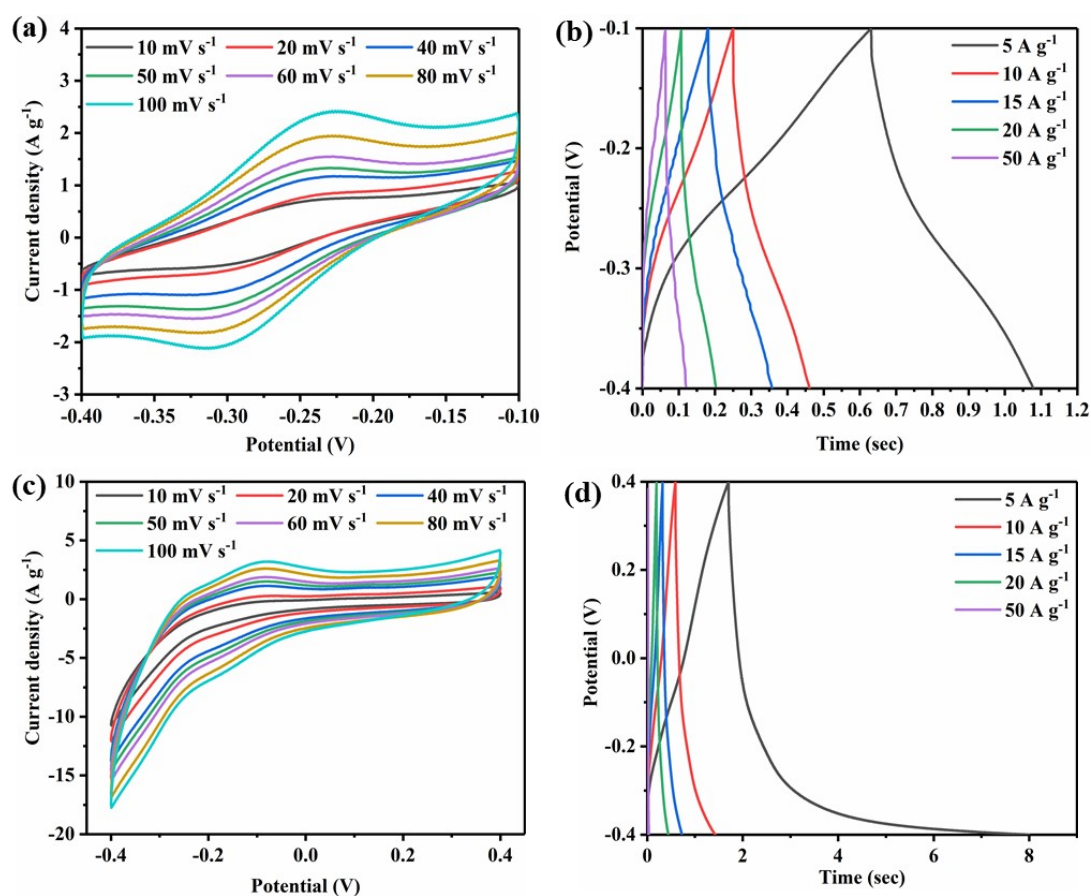


**Figure S1** (a) CV curves and (b) Galvanostatic charge–discharge curves of the working electrode with the mass ratio 8:1:1 of PIBQ polymer, carbon black, PVDF; (c) CV diagram and (d) Galvanostatic charge–discharge curves of the working electrode with the mass ratio 3:4:3 of PIBQ polymer, carbon black, PVDF.

## 6. Peak current diagram and capacitive contribution of PIBT-1%rGO composite

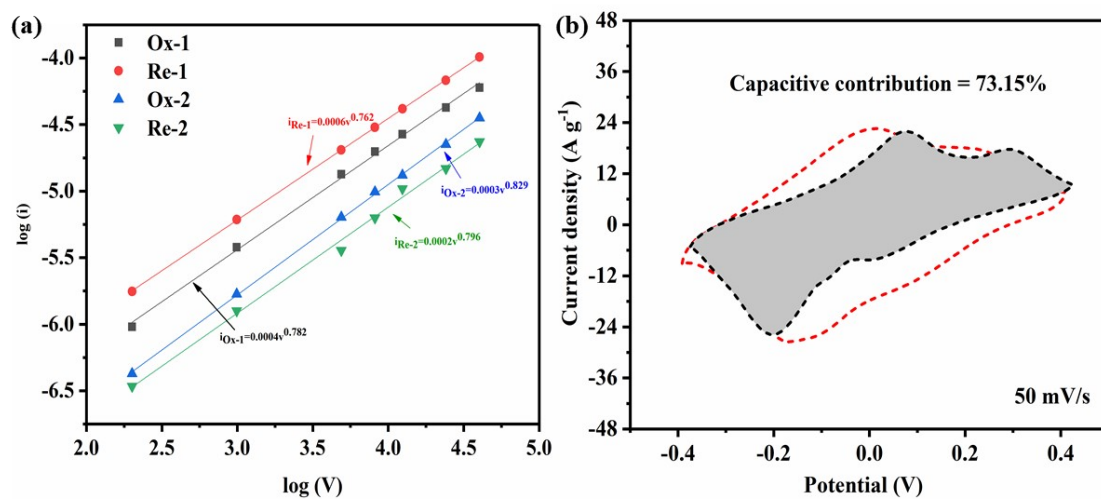


**Figure S2** (a) Scanning peak current diagram of PIBQ-1%rGO composite; (b) Capacitive and diffusion-controlled contributions to charge storage of PIBQ-1%rGO composite at 50  $mv\ s^{-1}$ .

## 7. Cycling stability of PIBQ-1%rGO composite

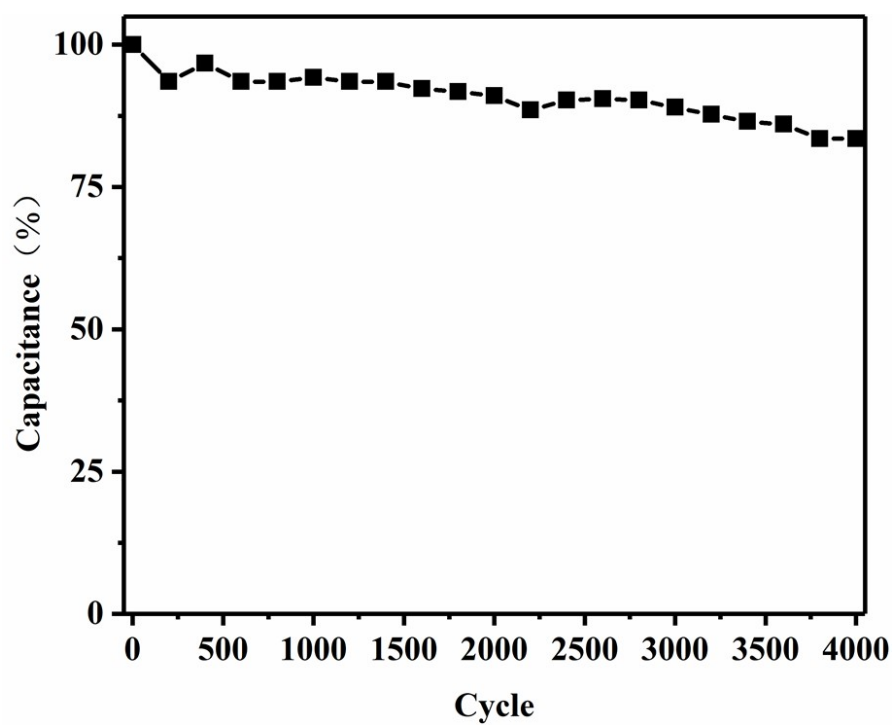


Figure S3 Cycling stability of PIBQ-1%rGO at a current density of 10 A g<sup>-1</sup>.



## 8. FT-IR characterization of PIBT-1%rGO composite

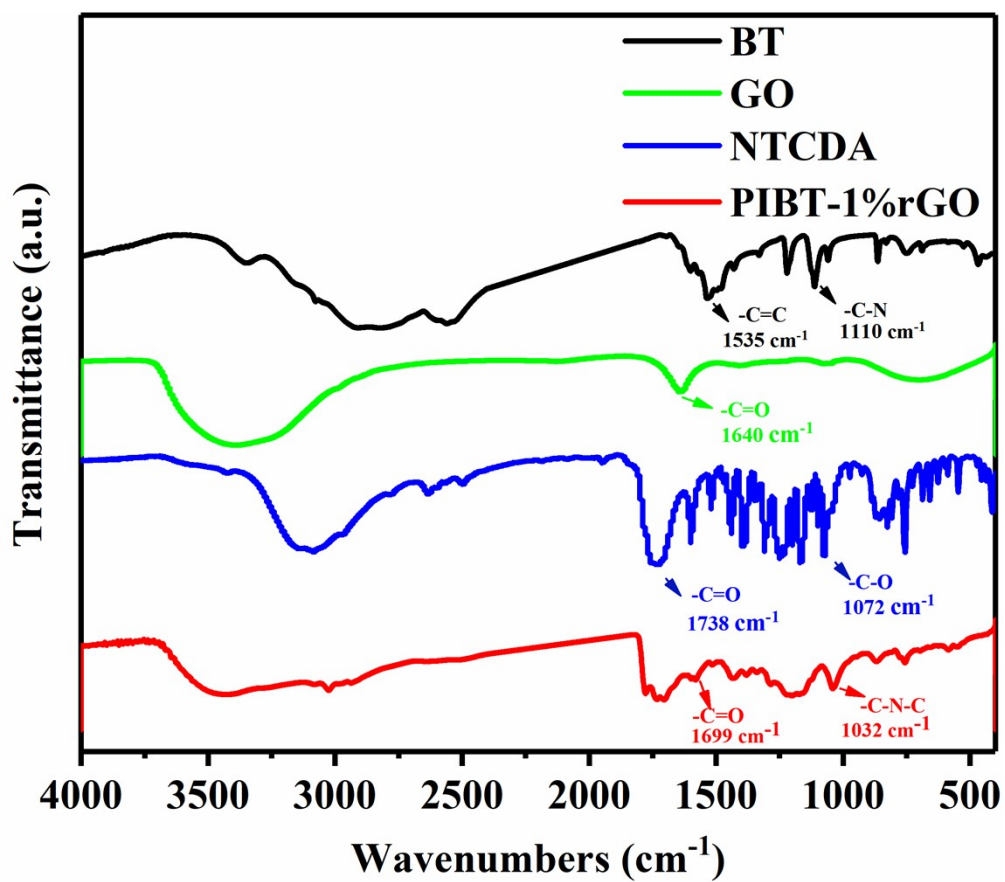


Figure S4 FT-IR spectra of BT monomer, GO, NTCDA monomer and PIBT-1%rGO polymer.

9. EIS diagram of PIBQ polymer, PIBT-1%rGO and PIBQ-1%rGO composites

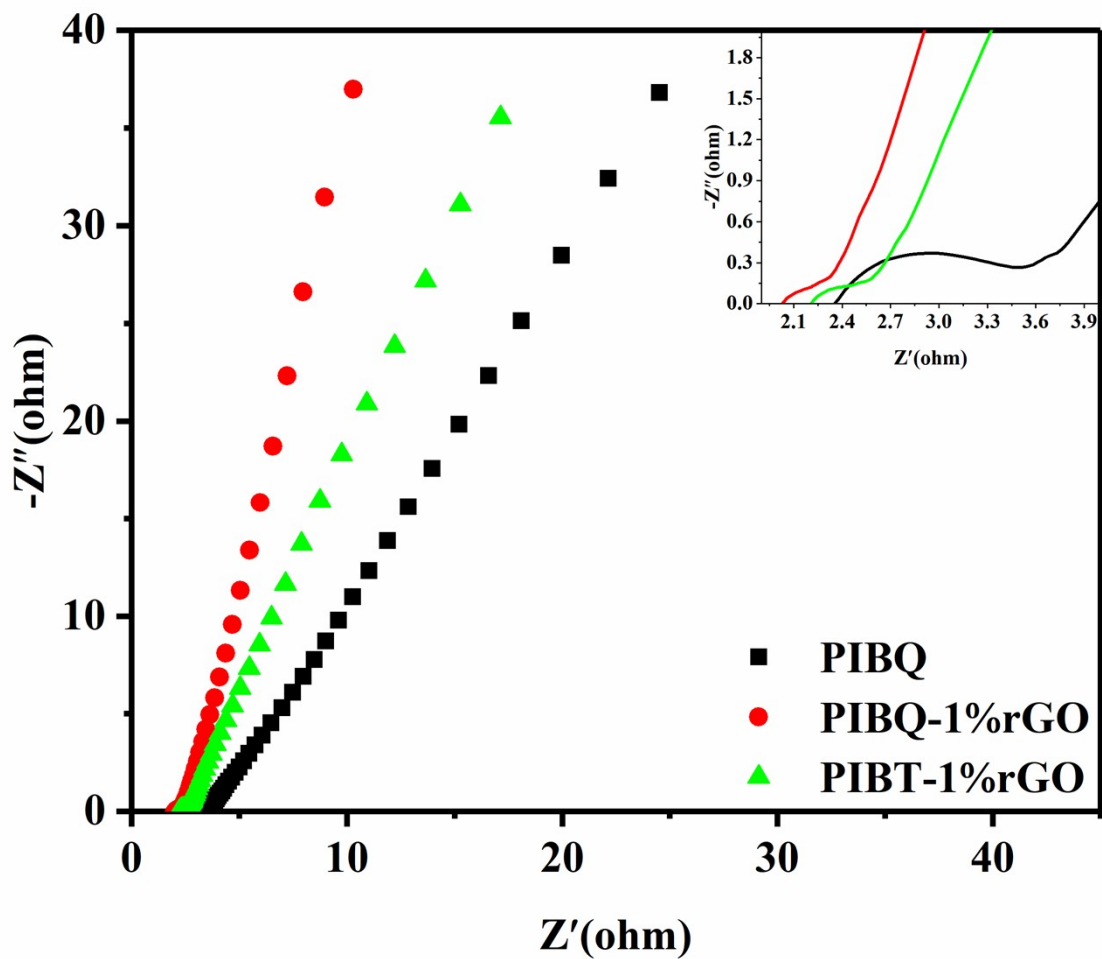
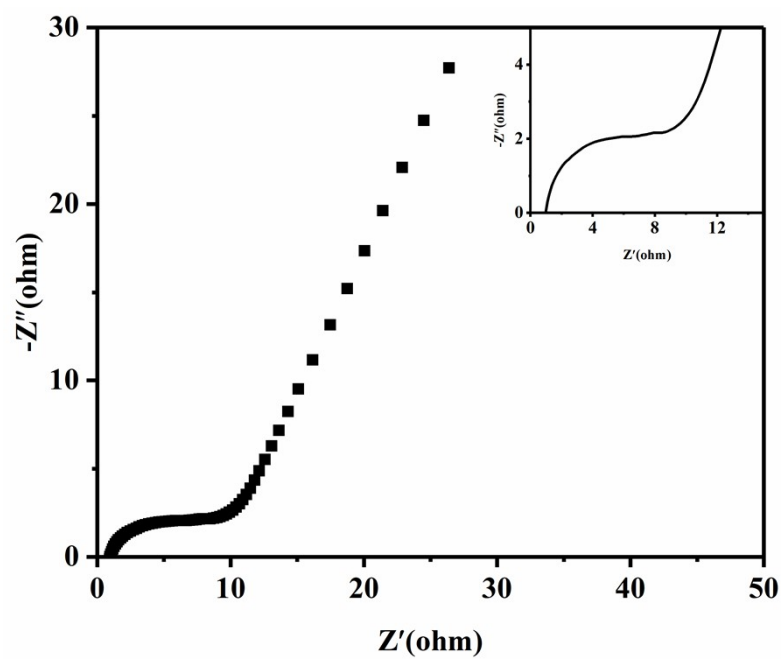


Figure S5 EIS diagram of PIBQ polymer, PIBT-1%rGO and PIBQ-1%rGO composites.

### 10. EIS diagram of PIBQ-1%rGO//PIBQ-1%rGO device



**Figure S6** EIS diagram of PIBQ-1%rGO//PIBQ-1%rGO symmetric device.

## 11. Reference

- [1] Luo, Z. Q.; Liu, L. J.; Ning, J. X. A Microporous Covalent–Organic Framework with Abundant Accessible Carbonyl Groups for Lithium-Ion Batteries. *Angew. Chem. Int. Ed.* **2018**, *57*, 9443–9446.